Available online at www.sciencedirect.com
ScienceDirect
Journal of Solid State Chemistry 180 (2007) 2377–2385
JOURNAL OF SOLID STATE CHEMISTRY
www.elsevier.com/locate/jssc

In situ and time resolved study of the γ/α-Fe_2O_3 transition in nanometric particles

T. Belin[a,*], N. Millot[b], N. Bovet[b], M. Gailhanou[c]

[a]*LACCO, UMR 6503 CNRS—Université de Poitiers, 40 Av. Recteur Pineau, F-86022 Poitiers cedex, France*
[b]*Institut Carnot de Bourgogne, UMR 5209 CNRS—Université de Bourgogne, 9 Av. A. Savary, BP 47870, F-21078 Dijon cedex, France*
[c]*LURE, Université Paris Sud—Bât 209D, BP 34, F-91898 Orsay, France*

Received 26 February 2007; received in revised form 15 June 2007; accepted 18 June 2007
Available online 22 June 2007

Abstract

In situ and real-time study of the γ to α-Fe_2O_3 transition is carried out on the H10 beamline at LURE (France). γ-Fe_2O_3 particles are synthesized by soft chemistry. These particles have an average diameter evaluated by X-ray diffraction of 9 ± 1 nm and a specific surface area of $116\,m^2\,g^{-1}$. The size of produced α-Fe_2O_3 particles is determined by in situ and time resolved X-ray diffraction measurements at different temperatures. An amazing evolution of size with time is revealed: an abrupt doubling of the α-Fe_2O_3 particle size is observed whatever the heating temperature. Some assumptions are given in order to explain this phenomenon which implies at the same time surface energy, granulometric distribution and coalescence of particles.

Keywords: Phase transition; Nanometric particles; In situ X-ray diffraction; Maghemite

1. Introduction

Physical and chemical properties of nano-sized materials exhibit substantial differences from those of micron-sized materials. Some properties have been found to vary with particle size, one example being the grain size-driven phase transitions [1,2]. Phase transitions lead to very innovative materials since the resulting materials, stabilized by surface energy, paradoxically present both a high temperature structure and a very fine microstructure free from defects generally induced by the predominant entropy term at high temperature. These structural transformations in different nanoscale materials are reported by a large number of studies. Examples are nanocrystalline cubic $BaTiO_3$ whereas the stable phase is tetragonal in monocrystals [3,4], cubic Fe_2O_3 (instead of rhombohedral) [5], tetragonal ZrO_2 (instead of monoclinic) [6,7] and monoclinic Y_2O_3 (instead of cubic) [8]. The more complete study of such transitions with complete experimental [9] and theoretical [10] determination of both surface and bulk energies concerns the corundum/spinel transition in Al_2O_3 [11]. Both thermodynamic and kinetic principles that control these transitions in bulk materials are not really appropriate in smaller sizes. However, only few studies are interested in the knowledge of the first transition steps.

About the γ to α-Fe_2O_3 phase transition, Multani shows that, at nanometric scale, the Fe_2O_3 phase is amorphous up to a size of 5 nm, then the stable phase is γ-Fe_2O_3 (maghemite) up to 30 nm. For higher sizes, the stable phase becomes α-Fe_2O_3 (hematite) [12]. This point of view is in agreement with the thermodynamic approach developed by Navrotsky for alumina system [13]. In this case, γ-Al_2O_3 has a lower surface energy than α-Al_2O_3 and becomes energetically stable at surface area greater than $125\,m^2\,g^{-1}$. From literature data emerge several parameters conditioning the γ/α transition: this structural transformation is influenced by intergranular diffusion (as a limiting factor) [14–18], specific surface area [19,20] and critical size of the system [21,22]. Moreover, the γ-Fe_2O_3 particles are obviously transformed to hematite α-Fe_2O_3 at temperature between 523 and 873 K, depending on their previous history [23–25].

*Corresponding author. Fax: +33 5 49 45 37 79.
E-mail addresses: thomas.belin@univ-poitiers.fr (T. Belin), nadine.millot@u-bourgogne.fr (N. Millot).

0022-4596/$ - see front matter © 2007 Elsevier Inc. All rights reserved.
doi:10.1016/j.jssc.2007.06.013

The novelty of this study is the time resolved following of γ to α-Fe_2O_3 transition occurring at the nanometric scale. Compared to classical in situ step by step methods which are often used to determine experimental transition temperature or resulting phases, the evolutions of both coherent diffraction domains and phase ratios are followed during the transition with a rate of one XRD pattern every 30 s. Combining our data with the literature data allows us to establish some mechanisms of the γ/α-Fe_2O_3 phase transition which remains still unknown in nanocrystals.

2. Experimental

2.1. Synthesis and preliminary characterizations

γ-Fe_2O_3 nanoparticles, homogeneous in size and oxygen stoichiometry, are prepared by soft chemistry using coprecipitation of cation precursors $FeCl_3 \cdot 6H_2O$ and $FeCl_2 \cdot 4H_2O$ by addition of an ammonia solution [14,26]. The solution is then centrifugated and washed to eliminate chloride impurities. The centrifugation/wash cycle is pursued until "sol" appearance. A freeze-drying process allows us to collect a highly divided powder. All powders are submitted to a thermal treatment in order to eliminate remaining impurities and to produce γ-Fe_2O_3 nanoparticles (all remaining Fe^{2+} cations are oxidized in Fe^{3+}). The conditions of the thermal treatment are determined by the control of four parameters: elimination of remaining impurities, control of oxygen stoichiometry, control of crystallite size and prevention of the transition between γ- and α-Fe_2O_3 forms. Samples are inserted at room temperature in a tubular furnace, heated at $2\,K\,min^{-1}$ up to 523 K under air atmosphere, and then kept in furnace for 4 h. Maghemite samples are then cooled rapidly to room temperature.

Chloride ions coming from the synthesis precursors were totally removed during washing and heat treatment of samples. X-ray photoelectron spectroscopy is very sensitive to the surface compounds and no contribution related to chloride ions (Cl 2*s* or 2*p*) is detected on spectra. Moreover, after washing treatment, iron oxide powders were submitted to controlled rate thermal analysis coupled with mass spectrometry (Pfeiffer Prisma QMS200). The heating rate ($2\,K\,min^{-1}$ by default) is adjusted in such a way that the rate of desorption can be constant in the temperature range of 298–873 K [27]. The chloride ions amount remains lower than the spectrometer detection limit (about 1×10^{-12} mbar and sensitivity for Argon: 10^{-4} A/mbar).

Many techniques such as X-ray diffraction and surface area measurement have been used to establish the cristallinity and the purity of the γ-Fe_2O_3 samples as described elsewhere [26]. The nanoparticles of maghemite γ-Fe_2O_3 used for these experiments have an average diameter evaluated by X-ray diffraction of 9 ± 1 nm and a specific surface area of $116\,m^2\,g^{-1}$. The XRD pattern could be indexed on the basis of the unit cell corresponding to the $P4_132$ space group, which suggest that the vacancies of the γ-Fe_2O_3 sample are perfectly ordered [28]. Deviation to the oxygen stoichiometry for this sample, inferred from the lattice parameter ($a = 0.8349$ nm), is equal to the one in maghemite ($\delta = 0.11$). High resolution electronic transmission micrograph of nanocrystalline γ-Fe_2O_3 powder (Fig. 1) shows nearly monodisperse and quasi-spherical shapes.

2.2. Quantitative measurements of γ/α-Fe_2O_3 transition parameters at LURE

The objective is to clear up the mechanisms of this phase transition at nanometric scale and low temperature. Various parameters involved in the γ/α transition are needed like evolutions of both the particle size and the phase ratio. The γ/α-Fe_2O_3 transition is thermally induced and the quantitative measurements are carried out using the LURE synchrotron XRD and X-ray absorption beamline facility (H10) during an isothermal heat treatment of nanosized γ-Fe_2O_3 powder.

At LURE, a real-time and in situ equipment allows us to measure XRD patterns with a good signal/noise ratio and a rate of one XRD pattern every 30 s. The monochromator is tuned to a radiation wavelength of $\lambda = 0.175361$ nm. Nevertheless, accurate quantitative measurements require several preliminary stages: the measurement of the instrumental resolution are necessary to obtain the α-Fe_2O_3 crystallites size in the powder from the XRD patterns during the heat treatment.

The instrumental resolution is determined using a reference material α-Al_2O_3. Thus, the broadening observed is not a size or distortion effects related to material. The instrumental resolution curve is shown in Fig. 2 and reveals a significant integral width mainly due to the beamline second mirror focussing. This one has a kapton window contributing in a significant way to the increase of the integral width. However, the particle size of γ-Fe_2O_3 powder determined in the furnace on the LURE equipment (9 ± 1 nm in diameter) is similar to the value obtained on the same powder at our laboratory without furnace.

The normal way of obtaining quantitative measurements of the γ/α-Fe_2O_3 transition is to use the interrelationships between diffracted intensities and chemical compositions

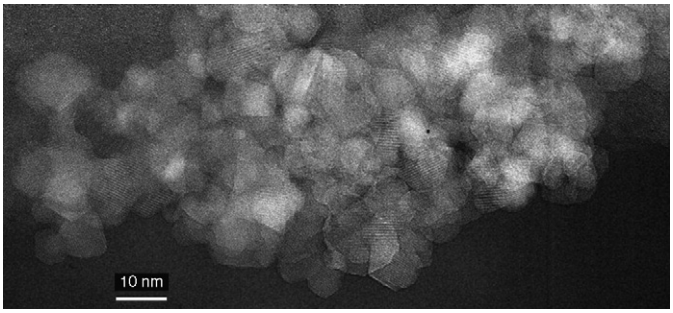

Fig. 1. HRTEM micrograph of quasi-spherical shape nanocrystalline γ-Fe_2O_3 powder used for in situ XRD experiments.

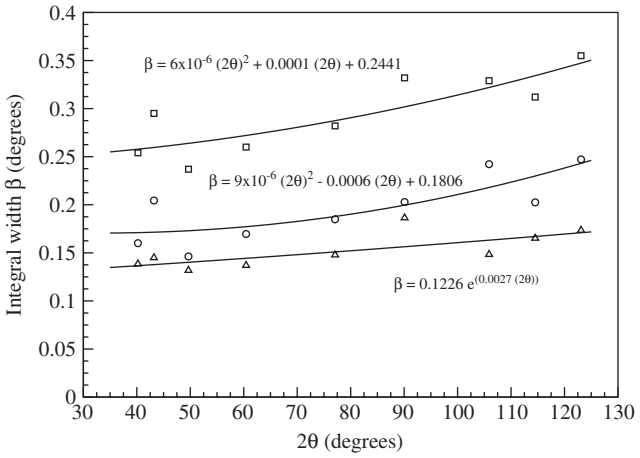

Fig. 2. A reference material (α-Al_2O_3) allowed the measurement of the instrumental resolution curve of the H10 beamline at LURE (France) with the furnace used for in situ experiments. This curve is applied to the analysis of experimental XRD peaks (from top to bottom: instrumental resolution curve, Lorentzian and Gaussian contribution).

of the phases. The mass absorption coefficients for γ- and α-Fe_2O_3 phases are the same ($\mu_e = (\mu/\rho) = 54.18\,cm^2\,g^{-1}$). Thus, the ratio of relative intensities allows directly a quantification. However, the most intense peak of maghemite (3 1 1) is unfortunately overlapped by the (1 1 0) hematite peak. In order to avoid overlapping problems, hematite (1 0 4) peak (relative intensity: 100) and maghemite (2 2 0) peak (relative intensity: 35) are used for quantitative measurements.

Samples of pure maghemite γ-Fe_2O_3 are laid out in a carry-sample of 0.4 mm depth. The kapton window of the furnace allowing X-rays beam through is cooled by water circulation. The accuracy of the measured temperature is estimated to be ± 15 K.

During the γ/α transition, the diffraction lines corresponding to α-Fe_2O_3 (higher index) appear jointly with the vanishing of the γ-Fe_2O_3 lines (lower index) (Fig. 3). Thus, the temperature is maintained until the complete transition of γ into α-Fe_2O_3 or more precisely until the vanishing of the maghemite peaks on XRD patterns. At the end of the measurement, only 2% maximum of maghemite phase remains into the samples.

Temperatures and ramps used are summarized in Table 1. Three identical powders named N1–N3 are heated, respectively at 623, 723 and 773 K. For each experiment, XRD patterns are recorded every 30 s, beginning at a temperature of 473 K.

Three methods, which are described in appendix, have been used to determine the α-Fe_2O_3 phase proportion from XRD patterns: modified internal standard (ISM), statistical and Rietveld methods. Patterns decomposition is carried out using the program PROFILE (available in the PC software DIFFRAC AT supplied by Siemens) and the Rietveld method using the XND 1.22 software [29]. Pseudo-Voigt peak profile analysis, using the Langford method, is performed to determine the average crystallite

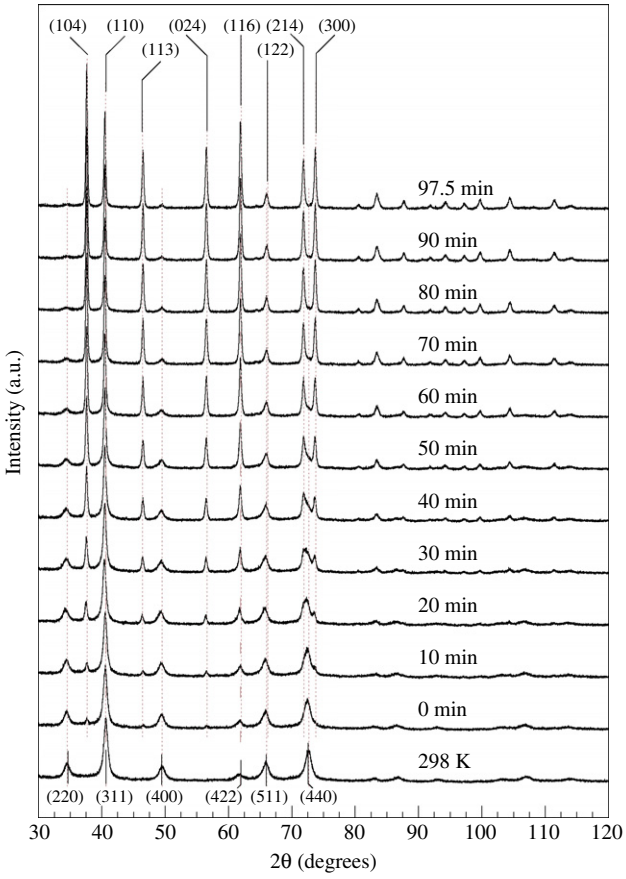

Fig. 3. Structural evolutions of γ-Fe_2O_3 sample during the γ/α phase transition at 723 K. Time is arbitrarily set to zero when α-Fe_2O_3 phase is detected. The lower and higher index are, respectively, related to γ- and α-Fe_2O_3. The shift due to the temperature between the 298 and 723 K on XRD patterns is detected but not visible on this reduced figure.

size (size of a region over which the diffraction is coherent) [30,31]. The powder lattice parameters are deduced from XRD line positions using a least-squares refinement method with an homebuilt software [32].

3. Results

Of all the experiments, only the first one (at about 623 K) does not present any modification even after 5 h. Obviously, the temperature is too low or the kinetic is too slow to allow the phase transition. The two successful experiments at about 723 and 773 K present the same evolutions. The size of the coherent domains of diffraction for each phase is measured on these XRD patterns (Fig. 4). The values obtained at 723 and 773 K prove, in both cases, a regular increase of the size of hematite particles with time: the lowest size detected is of 2 ± 1 nm. A maximum size of 90 ± 1 nm is reached at the end of the experiments. An abrupt upshift is observed on both experiments when the size of hematite particles is about 9 nm. In addition, there is no significant modification of the γ-Fe_2O_3 particles size.

Table 1
Temperatures and ramps applied to the pure γ-Fe_2O_3 samples to study by XRD the γ/α transition

Samples	Temperature ($K \pm 15$ K)	Temperature ramp (K min^{-1})		α-Fe_2O_3 detected
		From 298 to 473 K	Above 473 K	
N1	623	2	2	No (even after 5 h)
N2	723	2	2	Yes
N3	773	4	2	Yes

These measurements were performed on H10 beamline at LURE. Samples were synthesized by soft chemistry and the particle size was determined by XRD (about 9 nm).

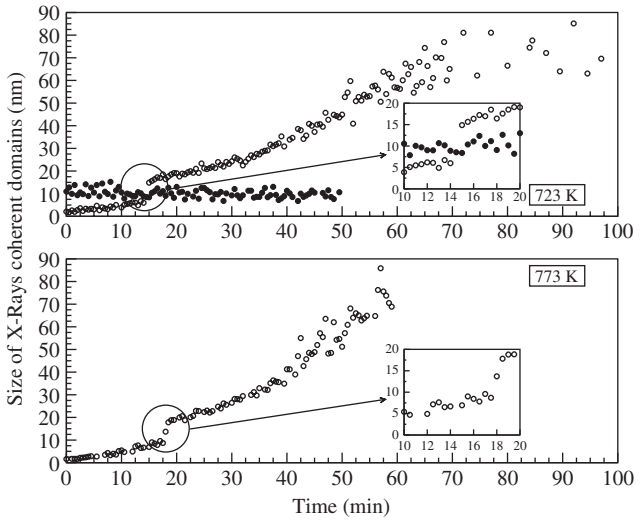

Fig. 4. Size of X-rays coherent domains of α-Fe_2O_3 (empty circle) and γ-Fe_2O_3 (black circle) phase during the γ/α transition. Maghemite γ-Fe_2O_3 samples (particle size of about 9 ± 1 nm) were heated at 723 and 773 K. A brutal increase of the X-rays coherent domain sizes (9–18 nm) was detected (see enlargement).

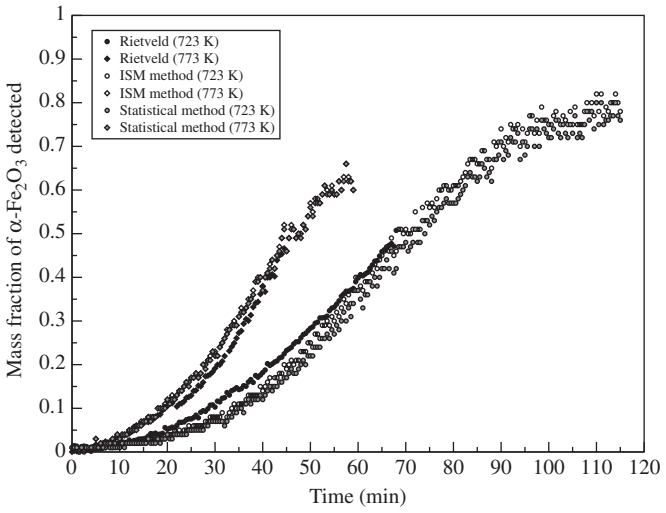

Fig. 5. Mass fraction of α-Fe_2O_3 detected within the γ-Fe_2O_3 phase during the γ/α transition at 723 K (methods used in determination of hematite proportion—white circles: modified ISM; gray: statistical method; black: Rietveld method) and at 773 K (white lozenge: modified ISM; gray: statistical method; black: Rietveld method). These curves are very similar to those obtained by Schimanke [21].

The weight fraction of α-Fe_2O_3 formed is given Fig. 5. A proportion of 50% weight of α-Fe_2O_3 is reached in 45 min in the case of the 773 K experiment instead of 70 min at 723 K. Above 50% weight, the dispersion of the observed domain sizes suggests a wide granulometric distribution (Fig. 4). The evolution versus time is very similar to the results observed in literature [21]. Whatever the methods of determination used (modified ISM, statistical or Rietveld methods), the weight fraction of hematite remains close up to 50%.

A refinement of these curves is possible by using a first-order kinetic relation defined as $x_\alpha = A(\exp(k_n t) - 1)$ where x_α is the weight fraction of hematite, t the time in seconds, k_n the rate constant (s^{-1}) and A a constant. The results of these refinements are given in Table 2. In a logical way, the rate constant is increased by the temperature (1.44×10^{-7} s^{-1} at 563 K up to 6.72×10^{-4} s^{-1} at 723 K and 8.66×10^{-4} s^{-1} at 773 K). The good refinement of the Rietveld method is confirmed by the low values of uncertainties obtained. It should be noticed that the

Table 2
Rate constants of the γ/α-Fe_2O_3 transition determined by refinement of the curves of the mass fraction (Fig. 5) using the relation $x_\alpha = A(\exp(k_n t) - 1)$

Method	Rate constant k_n (s^{-1})
Schimanke (563 K)	$1.44 \times 10^{-7} \pm 0.16 \times 10^{-7}$
Schimanke (583 K)	$8.30 \times 10^{-7} \pm 0.77 \times 10^{-7}$
Schimanke (603 K)	$1.70 \times 10^{-6} \pm 0.11 \times 10^{-6}$
Rietveld (723 K)	$4.83 \times 10^{-4} \pm 0.41 \times 10^{-4}$
Modified ISM (723 K)	$6.32 \times 10^{-4} \pm 0.70 \times 10^{-4}$
Statistical (723 K)	$5.92 \times 10^{-4} \pm 0.58 \times 10^{-4}$
Rietveld (773 K)	$8.66 \times 10^{-4} \pm 0.80 \times 10^{-4}$
Modified ISM (773 K)	$6.60 \times 10^{-4} \pm 0.83 \times 10^{-4}$
Statistical (773 K)	$6.72 \times 10^{-4} \pm 0.85 \times 10^{-4}$

Data obtained by Schimanke [21] are also reported. All values are given on the assumption of first-order kinetics.

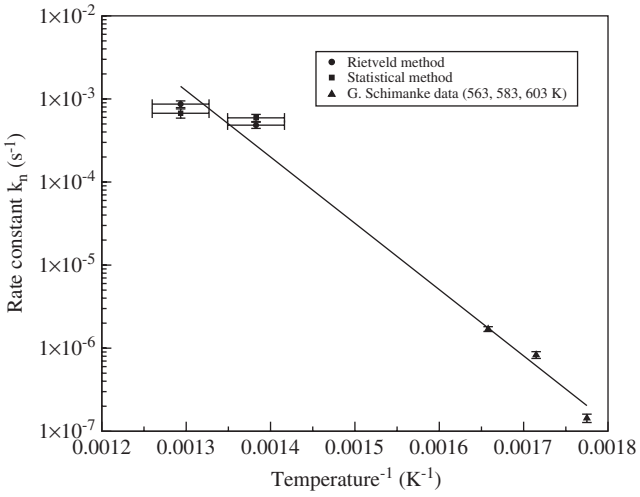

Fig. 6. Arrhenius diagram used to determine the activation energy of the γ/α-Fe_2O_3 phase transition (circle: our results at 723 and 773 K obtained at LURE; triangle: Schimanke data [21] at 563, 583 and 603 K for experiments during 150 h in this case).

modified ISM and statistical methods have also similar values of uncertainties. The small divergence observed can be explained by the slightly different shapes.

The γ/α transition activation energy is given by the well-known relation of Arrhenius: $k = k_0 \exp(-E_a/RT)$ where k is the rate constant (s^{-1}), k_0 a constant, E_a the activation energy ($J\,mol^{-1}$), R the gas perfect constant ($8.31418\,J\,K^{-1}\,mol^{-1}$) and T the temperature in Kelvin. The activation energy is found to be of about $176 \pm 31\,kJ\,mol^{-1}$ by Schimanke [21]. A precise activation energy cannot be determined using our results at 723 and 773 K due to possible error in the temperature. However, by joining our results to those of Schimanke [21] and using a linear regression, we can obtain an approximative value (about $152 \pm 17\,kJ\,mol^{-1}$): this confirms the coherence of the information obtained at LURE (Fig. 6).

4. Discussions

4.1. Mechanism assumptions of the phase transition

With these various results, we tried to submit a mechanism for the γ/α-Fe_2O_3 phase transition occurring at the nanometric scale. Previously, it is necessary to summarize the parameters which are involved in the phase stabilization. When a material exist under two phases A (at low temperature) and B (at high temperature), the conditions of the transition could be modified by the contribution of the free surface energy. This latter is also related to the particle size [33–35]. Thus, the decrease of the particle size should make possible to obtain at room temperature the usual stable phase of the infinite crystal known at high temperature. The illustration of this approach was obtained by McHale [9] on nanoparticles of alumina system (α-Al_2O_3 corundum and γ-Al_2O_3 spinel). The α phase is normally stable for an infinite crystal at 298 K. Molecular dynamic simulations of this system [10] show that the α phase surface energy can take rather different values ranging between 2.0 and $8.4\,J\,m^{-2}$. These values depends (i) on surface crystallographic orientation, (ii) on possible surface reconstruction, and (iii) on quantity of chemically adsorbed water on the surface. Concerning the γ phase, the surface energy values calculated are in the range of 0.8–$2.5\,J\,m^{-2}$. As a consequence, γ phase has a surface energy smaller than α phase. Thus, for high specific surface area (above $125\,m^2\,g^{-1}$), this phase is stable (minimization of the total energy of the material) [36].

Similar to alumina transition, the maghemite γ-Fe_2O_3 to hematite α-Fe_2O_3 transition can be explained using the same concepts. γ-Fe_2O_3 is stable for the lowest grain sizes and α-Fe_2O_3 for the coarse ones. Therefore, the coalescence of the γ-Fe_2O_3 particles, induced by the diffusion of cations during the heat treatment, is necessary for the appearance of α-Fe_2O_3 structure. This increase of γ-Fe_2O_3 particles size is not clearly observed in Fig. 4 (only few points at the beginning of the experiment is above 15 nm). This can be explained by the fact the transition size is around this value of 15 nm and by the small amount of transited grains (less than 5%: see Fig. 5). But an interesting feature remains: an abrupt upshift is observed between 10 and 20 min after detection of the first α-Fe_2O_3 domains. The size of coherent domains increases from 9 nm (similar to the crystallite size of maghemite γ-Fe_2O_3) up to 18 nm. Why this doubling of size? Using the real-time and in situ data obtained at LURE, it is possible to propose two mechanisms for the γ/α transition in nanometric grains.

4.1.1. Germination–growth model: an usual mechanism for coarse grains

In the case of alumina transition observed in micrometric grains, the thermally activated transition implies nucleation of germs on high energy sites like dislocations, grain boundaries, stacking faults or impurities [37]. This nucleation is followed by the germs grown until the transition is complete: the atoms reordering leads to the modification of the crystalline structure. In addition, thanks to microtomies on γ alumina grains partially transformed (size of about 5.5 μm), Tucker [38] and Dynys [39] showed the α phase nucleation begins preferentially on the surface from or near the curve inversion when two particles are sintered.

In the case of the γ-Fe_2O_3 nanoparticles used in this study, several remarks can be made: (i) surface is a favorable place with the presence of "high" energy sites [28]; (ii) there is no presence of intragranular boundaries due to the fact that the nanoparticles are not polycrystalline [28]; (iii) the coherent size domains of the α-Fe_2O_3 phase grows continuously until reaching the γ-Fe_2O_3 particle size, then this size is doubled (Fig. 4). This is incompatible with a nucleation near the curve inversion since, in this case, the α-Fe_2O_3 germ should grow continuously, in at least two grains, up to the value of

18 nm approximately (twice the size of initial γ-Fe_2O_3 particles considering the system in one direction). In the case of nucleation near the curve inversion, the size jump could not be explained.

By analogy with alumina, a surface nucleation of α-Fe_2O_3 should be considered (Fig. 7a). Indeed, in XRD, the smallest size of coherent domains detected (about 2 nm) could be a proof of this nucleation. α-Fe_2O_3 germs grow in the grains and finally gives only one particle. This would explain the size gap in the coherent domains from 9 to 18 nm (Fig. 4, circles). Nevertheless, in this case we should draw the assumption that the initial two α-Fe_2O_3 germs are finally replaced by only one using an epitaxy phenomenon or a lattice reorganization to minimize lattice energy. Then, particles would continue to grow until reaching a size of 60–80 nm by intergranular sintering. In this scheme, germs of α-Fe_2O_3 with a size ranging from 2 to 18 nm have been observed. However, the α phase is normally stable only for grain size above 20 nm as shown in literature [5,13,14]. This result is not in contradiction with thermodynamics. Indeed, it is already proved that the stabilization of nanometric structures depends on the nature of the external interface [14,40]. In this case, the α-Fe_2O_3 coherent domains, smaller than 18 nm, are located in the maghemite particles with solid/solid interfaces. The interface energy is then smaller and could lead to the stabilization of these α germs.

This mechanism is not free from inconsistencies. Indeed, during the growth of α-Fe_2O_3 in the grain, a size reduction of the maghemite γ-Fe_2O_3 coherent domains should be observed: this is not clearly measured (Fig. 4, black circles). However, this could be explain if we assume that the peak used in the size determination is more sensitive to the biggest coherent domains. Taking into account the γ-Fe_2O_3 proportion already transformed, a size distribution of diffraction coherent domains should be calculated in order to prove this assumption. In addition, crystalline coherence between the hematite which grow in several particles or crystalline rearrangement have to be proven.

4.1.2. Another possible mechanism for nanometric grains

Another interpretation of results of real-time XRD patterns can be given. Initially, the assumption of a coalescence of γ-Fe_2O_3 particles can be preserved: the decrease of specific surface area explains the appearance of α-Fe_2O_3. However, the maghemite powders are not perfectly monodisperse (Figs. 7b and 1). There is a granulometric distribution centered on a maximum at 9 nm. Successive steps of γ/α transition are then possible: particles with a size smaller than 9 nm (less than 10% according to the Figs. 4 and 5) would be transformed first because of their higher reactivity. In the volume of these small particles, transition to α phase would be thus quasi-instantaneous. Then the main part of particles (corresponding to the maximum of the granulometric distribution: 9 nm) would be transformed and this would lead to the brutal gap of the coherent domains of size observed in Fig. 4 (gap from 9 to 18 nm). Growth of the hematite particles would be obtained by intergranular sintering. However, like the previous mechanism, this one suffers from some inconsistencies compared to results in the literature. Hematite particles of about 2 nm in size implies the stability of this structure for such small particles. Without the presence of a solid/solid interface, this stability would be difficult to achieved [14].

4.1.3. Is the γ/α-Fe_2O_3 transformation, induced by crystals size modification, a true phase transition?

In physics, a phase transition is the reversible transformation of a thermodynamic system toward another. In the case of phase transitions induced by crystals size, confusion comes owing to the fact that the evolution of grains size is in general obtained by increasing the temperature. It is the way to pass from γ-Fe_2O_3 to α-Fe_2O_3. When the temperature is reduced, one does not decrease the crystals size, consequently the α phase remains, it is no more possible to obtain the γ phase again. The non-reversability of this transformation is not a proof to conclude that it is

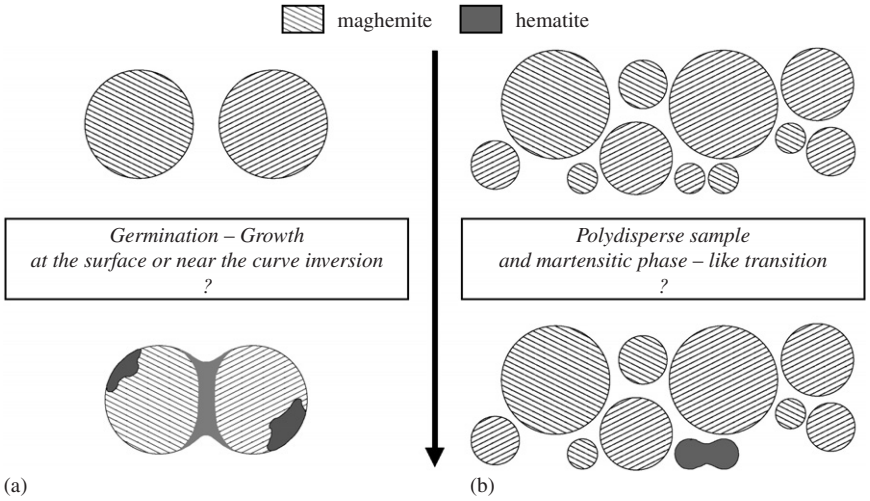

Fig. 7. Different mechanisms proposed for the γ/α-Fe_2O_3 transition at nanometric scale: (a) monodisperse γ-Fe_2O_3 sample and germination–growth process of the α phase; (b) polydisperse γ-Fe_2O_3 sample and martensitic phase-like transition.

not a phase transition. Indeed, the parameter which it is advisable to modify is not the temperature but the grain size. For example, when Randrianantoandro crushes with high energy α-Fe_2O_3 powder, he demonstrates that one can induce the reverse transition [22]. At the time of crushing, the size of α-Fe_2O_3 grains decrease, until obtaining the stable phase for high specific surfaces: $\gamma - Fe_2O_3$. It thus acts well that γ/α transformation is a real-phase transition.

5. Conclusions

In situ and real-time study of γ to α-Fe_2O_3 transition has been carried out on the H10 beamline at LURE (France). The size of produced α-Fe_2O_3 particles has been determined by X-ray diffraction measurements (lowest observed cristallites size: 2 nm). An amazing evolution of size with time is revealed: an abrupt doubling of the α-Fe_2O_3 particle size is observed whatever the heating temperature. Some assumptions have been given in order to explain this phenomenon which implies at the same time surface energy, granulometric distribution and coalescence of particles. According to the thermodynamic, the most probable way for this transition at nanometric scale is a germination–growth mechanism. More results would be obtained using techniques sensitive to very small coherent crystallographic domains such as HRTEM. Such investigations have already been realized in our team. However, the difficulty here is the observation of domains transformed which are not necessarily collapsed through the grain (all the depth of the sample is not necessarily transformed). Then, grains perfectly calibrated in size are required in order to definitively eliminate the second mechanism based on a martensitic phase-like transition of a powder with large grain-size distribution. Such sample can be obtained thanks to the thermal decomposition of iron pentacarbonyl in the presence of oleic acid, this study is also in progress [40].

Acknowledgments

The author would like to thank Dr. N. Floquet (CRMC2—Marseille, France), Pr. H. Van Damme (ESPCI—Paris, France), Pr. M. Pijolat (LPMG, St Etienne, France) for helpful discussions and Dr. E. Gauthier (IMN—Nantes, France) for TEM experiments.

Appendix A

Different methods were used to determine the proportion of each phase during γ/α-Fe_2O_3 transition. Some technical aspects are summarized in the following subsections:

A.1. Internal standard method

Using mixtures of γ- and α-Fe_2O_3 powders, a calibration curve could be established from XRD patterns. Various mixtures are realized using γ-Fe_2O_3 powder obtained by soft chemistry (diameter of 9 ± 1 nm) and commercial α-Fe_2O_3 powder (diameter of about 125 nm; AVX-TPC enterprise). These powders were crushed during 3 min in a mortar. Table A1 summarizes the mixtures used and Fig. 8 presents the resulting calibration curve.

A modified ISM is used to obtain the mass fraction of the α-Fe_2O_3 phase and to take into account the matrix effects present when a phase is diluted in another. For an homogeneous sample without preferential orientation (this is the case since we use quasi-spherical powders), without extinctions effect nor absorption, the intensity I_i of a peak corresponding to phase i is directly related to the weight fraction x_i of the phase and to the linear absorption coefficient μ_e of the sample through the relation:

$$I_i = \frac{x_i}{\mu_e k_i},$$

where k_i is a calibration constant. By considering the relation between weight fractions $x_\alpha + x_\gamma = 1$ and a sample made up of two phases with identical mass absorption coefficients, one can write in the case of a γ/α-Fe_2O_3 mixture (respectively for the (2 2 0) peak of γ-Fe_2O_3 and (1 0 4) of α-Fe_2O_3):

$$\frac{I_\alpha(1\,0\,4)}{I_\gamma(2\,2\,0)} = K\left(\frac{x_\alpha}{1 - x_\alpha}\right).$$

The constant K is determined from the reference mixtures. This method cannot be easily applied when no pure standards are available or when the crystallinity of both the standards and the compounds in the samples are different.

Table A1
Summary of γ/α-Fe_2O_3 mixtures realized in order to establish a calibration curve for in situ XRD experiments

	Specific surface area ($m^2\,g^{-1}$)	XRD size (± 1 nm)	Lattice parameter (± 0.0001 nm)	Mass (mg)					
α-Fe_2O_3	15	125	$a = 0.5035$ $c = 1.3749$	0.0	27.7	62.1	92.9	121.3	147.0
γ-Fe_2O_3	116	9	$a = 0.8349$	157.0	122.4	91.4	60.4	30.2	0
			α-Fe_2O_3 wt%	0	18.4	40.5	60.6	80.0	100

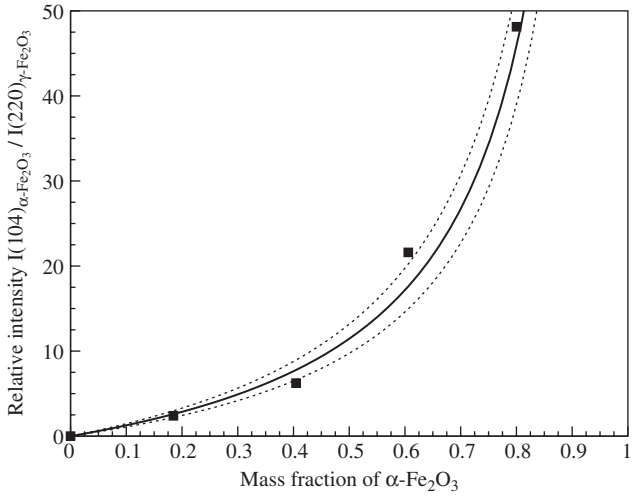

Fig. 8. Calibration curve used with modified internal standard method (ISM) to determine α-Fe_2O_3 proportion during the γ/α phase transition. The relative intensity ratio of (1 0 4) peak of α-Fe_2O_3 and (2 2 0) peak of γ-Fe_2O_3 is used to obtain the weight percentages of α-Fe_2O_3 in samples. Black boxes: experimental ratio for various mixtures defined in Table A1; black line: ISM approximation defined by $I(1\,0\,4)/I(2\,2\,0) = 11.447\,(x_{alpha}/(1 - x_{alpha}))$; dashed line: ±15% deviation of the refinement parameter.

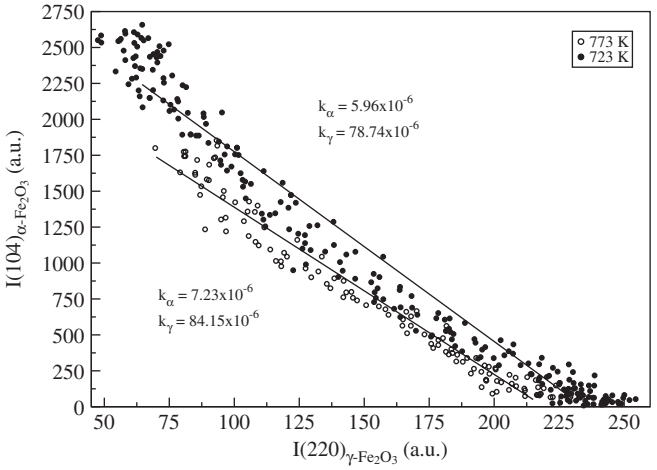

Fig. 9. Values of the calibration constants obtained from a linear least-square procedure on the intensity of the diffraction peak of γ-Fe_2O_3 and α-Fe_2O_3. Experimental data are given for the studied temperature of 723 and 773 K.

Moreover, for high intensities ratios (high mass percentage of hematite phase), the proportion of the measured phase is underestimated.

A.2. Statistical method

To avoid the use of a calibration curve which leads to some uncertainties, a statistical approach developed by Rius et al. [42] is also used. This method is based on the determination of calibration constants k_α and k_γ for α- and

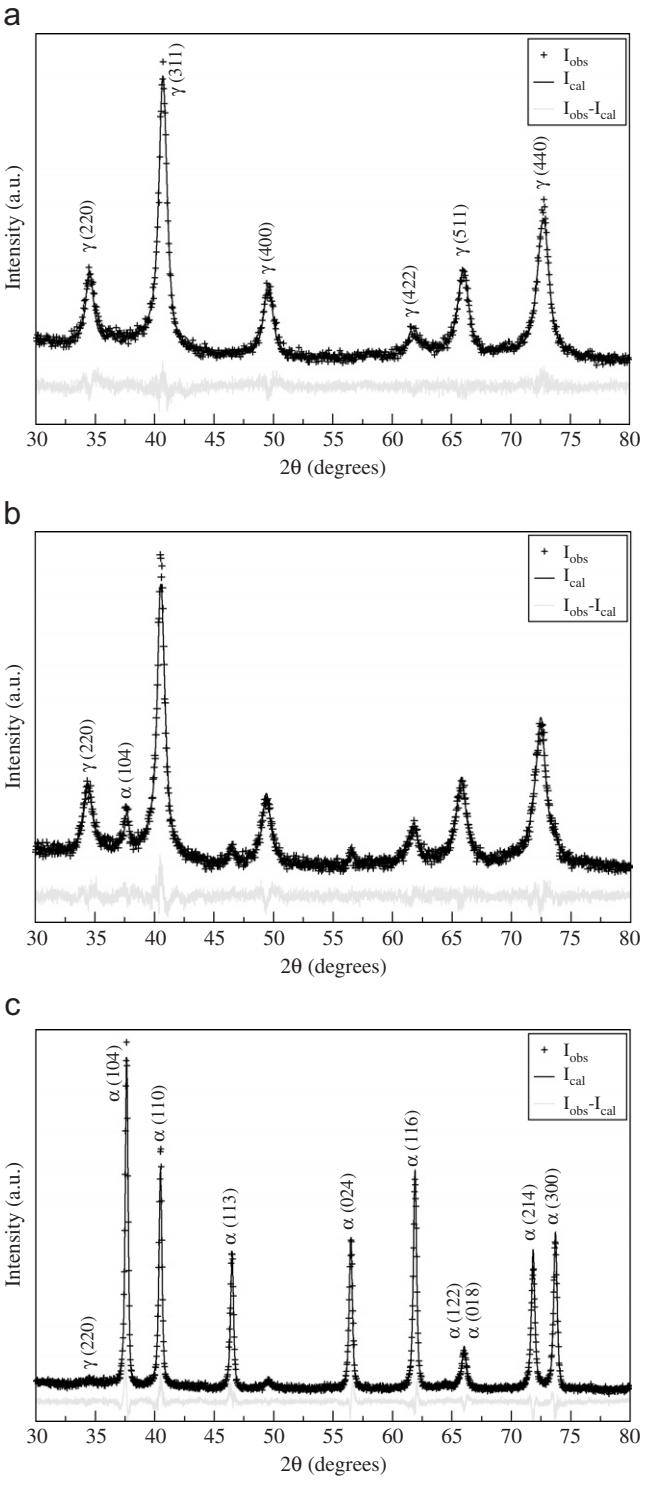

Fig. 10. Structural refinements of XRD patterns using the Rietveld method: (a) 0%, (b) 5% and (c) 98% of α-Fe_2O_3 phase in γ-Fe_2O_3 (refinement parameters for 0% [R_p: 0.0635; R_{wp}: 0.0803; R_{bragg}: 0.0236; GoF: 1.15], for 5% [R_p: 0.0779; R_{wp}: 0.0961; R_{bragg}: 0.0283; GoF: 1.38] and for 98% [R_p: 0.0780; R_{wp}: 0.0964; R_{bragg}: 0.0371; GoF: 1.37]). The use of scale factors allows to determine the proportion of α-Fe_2O_3. These XRD patterns were obtained at LURE during the γ/α transition (at about 723 K).

γ-Fe_2O_3 phases by the use of a conventional least-squares procedure. The experimental data and the values of the calibration constants are given for each temperature with

Fig. 9. The relation between intensity of the diffraction peak is the following:

$$I(1\,0\,4)_\alpha = \frac{1}{k_\alpha \mu_e} - \frac{k_\gamma}{k_\alpha} I(2\,2\,0)_\gamma$$

and, finally, we are left with the weight fraction of α-Fe_2O_3:

$$x_\alpha = \frac{k_\alpha I(1\,0\,4)_\alpha}{k_\alpha I(1\,0\,4)_\alpha + k_\gamma I(2\,2\,0)_\gamma}.$$

A.3. Rietveld method

Another alternative can also be considered: structural refinements are carried out on the XRD patterns (Figs. 10a–c) by using the Rietveld method of the software XND [29,43]. The α-Fe_2O_3 weight fraction x_α is given by the scale factor *Scale* of each phase through the relations:

$$S = \frac{\mu_\alpha V_\alpha^2 Scale_\alpha}{\mu_\gamma V_\gamma^2 Scale_\gamma},$$

$$x_\alpha = \frac{S}{1+S},$$

where μ is the absorption coefficient (cm^{-1}) of the considered phase and V the volume (nm^3) of the crystallographic cell [29,44]. The scale factor is an XND parameter used to refine the calculated diffracted intensities to the observed ones. The correlation of the scale factor with the α-Fe_2O_3 proportion is checked with the reference mixtures as defined in Table A1. Some refinement parameters are used to check the reliability of the fit: R_p and R_{wp} are residual factors which are respectively linear and minimized sum. These factors must be close and weak (about 0.1). The agreement between observed and calculated intensities is represented by R_{bragg} and should be lower than 0.1. GoF is the "goodness of fit" (ratio between residual and hoped factors) and its expected limit is 1.

References

[1] H. Gleiter, Nanostruct. Mater. 6 (1995) 3.
[2] R.W. Siegel, Nanostruct. Mater. 4 (1994) 121.
[3] S.S. Flashen, J. Am. Chem. Soc. 77 (1955) 6194.
[4] K. Uchino, E. Sadanaga, T. Hirose, J. Am. Chem. Soc. 72 (1989) 1555.
[5] P. Ayyub, M. Multani, M. Barma, V.R. Palkar, R. Vijayaraghavan, J. Phys. C. Solid State Phys. 21 (1988) 2229.
[6] R.C. Garvie, J. Phys. Chem. Soc. 77 (1978) 218.
[7] R.C. Garvie, M.F. Goss, J. Mater. Sci. 21 (1986) 1253.
[8] G. Skandan, C.M. Foster, H. Frase, M.N. Ali, J.C. Parker, H. Hahn, Nanostruct. Mater. 1 (1992) 313.
[9] J.M. McHale, A. Auroux, A.J. Perrotta, A. Navrotsky, Science 277 (1997) 788.
[10] S. Blonski, S.H. Garofalini, Surf. Sci. 295 (1993) 263.
[11] J.M. McHale, A. Navrotsky, A.J. Perrotta, J. Phys. Chem. B 101 (1997) 603.
[12] M.S. Multani, Conden. Matter News 1 (1991) 25.
[13] A. Navrotsky, Geochem. Trans. 4 (2003) 34.
[14] N. Millot, D. Aymes, F. Bernard, J.C. Niepce, A. Traverse, F. Bouree, B.L. Cheng, P. Perriat, J. Phys. Chem. B 107 (2003) 5740.
[15] J. Adnan, W. O'Reilly, Phys. Earth Planet. Inter. 110 (1999) 43.
[16] S. Mornet, F. Grasset, E. Duguet, Proceedings of the Eighth International Conference on Ferrites (ICF8), Kyoto, Tokyo, 2000, p. 766.
[17] C. Chaneac, E. Tronc, J.P. Jolivet, Nanostruct. Mater. 6 (1995) 715.
[18] C. Chaneac, E. Tronc, J.P. Jolivet, J. Mater. Chem. 6 (1996) 1905.
[19] B. Gillot, H. Nouaim, Mater. Chem. Phys. 28 (1991) 389.
[20] A. Rousset, G. Boissier, J.P. Caffin, Report of the Academy of Sciences of Paris, vol. 299, 1984, p. 781.
[21] G. Schimanke, M. Martin, Solid State Ionics 136–137 (2000) 1235.
[22] N. Randrianantoandro, A.M. Mercier, M. Hervieu, Mater. Lett. 47 (2001) 150.
[23] P. Cousin, P.A. Ross, Mater. Sci. Eng. A 130 (1990) 119.
[24] E. Herrero, M.V. Cabanas, M. Vallet-Regi, Solid State Ionics 101–103 (1997) 213.
[25] G. Ennas, G. Marongiu, A. Musinu, J. Mater. Res. 14 (1999) 1570.
[26] T. Belin, N. Guigue-Millot, T. Caillot, D. Aymes, J.C. Niepce, J. Solid State Chem. 163 (2002) 459.
[27] T. Panczyk, F. Villiéras, W. Rudzinski, M. Pelletier, A. Razafitianatiaharavo, Phys. Chem. Chem. Phys. 6 (2004) 3684.
[28] T. Belin, N. Millot, F. Vilieras, O. Bertrand, J.P. Bellat, J. Phys. Chem. B 108 (2004) 5333.
[29] J.F. Berar, G. Baldinozzi, IUCR-CPD Newsletters, vol. 20, 1998, p. 3.
[30] N.C. Halder, C.N.J. Wagner, Acta Crystallogr. 20 (1966) 91.
[31] J.I. Langford, National Institute of Standards and Technology: Accuracy in Powder Diffraction, 1992, p. 110.
[32] F. Bernard, F. Charlot, P. Sarrazin, J. Phys. IV 6 (1996) 103.
[33] J.W. Gibbs, Collected Works, vol. 1, New Haven, Yale, 1948.
[34] P. Perriat, J.C. Niepce, J. High Temp. Chem. Proc. 3 (1994) 585.
[35] P. Perriat, Nanostruct. Mater. 6 (1995) 791.
[36] A. Navrotsky, PNAS 101 (2004) 12096.
[37] D.S. Tucker, J. Am. Ceram. Soc. 68 (1985) 163.
[38] D.S. Tucker, E.J. Jenkins, J.J. Hren, J. Electron Microsc. Tech. 2 (1985) 29.
[39] F. Dynys, J.W. Halloran, J. Am. Ceram. Soc. 65 (1982) 442.
[40] N. Bernaben, A. Leriche, B. Thierry, Fourth Euro Ceram. 5 (1995) 203.
[40] T. Hyeon, S.S. Lee, J. Park, Y. Chung, H.B. Na, J. Am. Chem. Soc. 123 (2001) 12798.
[42] J. Rius, F. Plana, A. Palanques, J. Appl. Crystallogr. 20 (1987) 457.
[43] L.B. Mc Cusker, R.B. Von Dreele, D.E. Cox, J. Appl. Crystallogr. 32 (1999) 36.
[44] P. Suortti, J.B. Hastings, D.E. Cox, Acta Crystallogr. A 41 (1985) 413.